Unified Kinematic and Dynamical Modeling of a Soft Robotic Arm by a Piecewise Universal Joint Model

Zhanchi Wang, Gaotian Wang, and Nikolaos M. Freris

***Abstract*— The compliance of soft robotic arms renders the development of accurate kinematic & dynamical models especially challenging. The most widely used model in soft robotic kinematics assumes Piecewise Constant Curvature (PCC). However, PCC fails to effectively handle external forces, or even the influence of gravity, since the robot does not deform with a constant curvature under these conditions. In this paper, we establish three-dimensional (3D) modeling of a multi-segment soft robotic arm under the less restrictive assumption that each segment of the arm is deformed on a plane without twisting. We devise a kinematic and dynamical model for the soft arm by deriving equivalence to a serial universal joint robot. Numerous experiments on the real robot platform along with simulations attest to the modeling accuracy of our approach in 3D motion with load. The maximum position/rotation error of the proposed model is verified 6.7x/4.6x lower than the PCC model considering gravity and external forces.**

I. INTRODUCTION

The emergence of soft robotic arms provides many new perspectives for the application of robots [1] such as soft arms in interactive tasks [2], soft surgical robots [3], and soft artificial limbs [4]. Modeling soft arms is a challenging endeavor due to two main characteristics that are distinctive from rigid robots, namely: continuous deformation and 'infinite' passive degrees of freedom [5].

The most widely adopted assumption in modeling soft robotic arms is Piecewise Constant Curvature (PCC), which treats the arm as a concatenation of multiple segments each one being an arc of constant curvature [6], [7]. Several models for kinematics and dynamics of soft arms were developed based on PCC. A kinematic model of a planar soft arm was proposed in [8] and a dynamical model of a soft arm within a sagittal plane was developed in [9]. Della Santina et al. [10] cast a discrete joint robot analogue of a soft robot under PCC and established a two-dimensional dynamical model leveraging methods for rigid robots. This method was extended to three dimensions (3D) in [11], where a 10-joint rigid robot was used to imitate the motion of a single segment of the soft arm. However, there are discontinuities and singularities in the commonly employed state representation (direction/angle of bending) of PCC which limit the range of applicability of PCC based models [12]. An improved state representation of PCC was presented in [13], where four arcs are used as parametrization to represent one constant curvature segment to establish direct connection to physical quantities of soft robotic arms. A similar representation is used to derive a dynamical model of the soft arm in the 3D space [14].

Z. Wang and N. Freris are with the School of Computer Science and G. Wang is with the School of Physics; University of Science and Technology of China; Emails: zkdwzc,vectorwang@mail.ustc.edu.cn, nfr@ustc.edu.cn

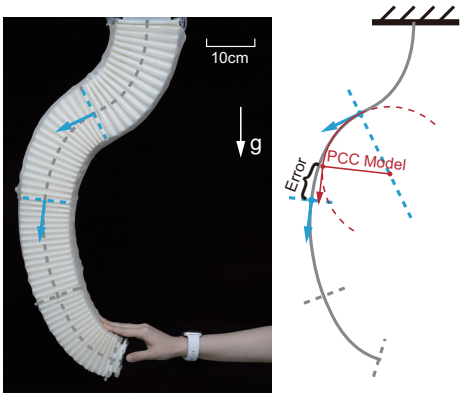

Fig. 1. A soft robotic arm interacting with humans. All segments violate the constant curvature assumption in this case; the second segment is illustrated as an example.

Although the PCC assumption is natural and advantageous in modeling, it fails to capture non-constant curvature deformation of the arm. As shown in Figure 1, when the soft arm interacts with the environment, all segments of the arm no longer deform in a constant curvature manner. In this case, the use of PCC to describe the arm will introduce modeling errors. As the number of segments increases, the errors accumulate and propagate to the end effector, thus deteriorating the fidelity of forward kinematics.

One approach is to describe a soft robot with a discrete-joint robot equivalent. The models in [11], [15] have the potential to cope with non-constant curvature deformation, but use PCC as an intermediate state representation; modeling becomes inaccurate when the arm does not deform in a PCC manner, e.g., operates under the effect of gravity.

In this article, we propose a new modeling method for soft robot arms, which capitalizes on a Piecewise Universal Joint (PUJ) principle. PUJ regards each segment of the soft arm as a universal joint whose links are stretchable. This method only assumes that *each segment of the arm is deformed in the same plane without twisting*. Comparing with PCC, PUJ relaxes the constraint that one segment of the arm must be deformed in a constant curvature manner and achieves a more general representation. We develop kinematic and dynamical models for the soft arm by utilizing rigid robot modeling under the PUJ principle. Our experiments unravel that the PUJ kinematic model demonstrates superior performance compared to the state-of-the-art PCC model in the presence of external forces. We also experimentally verified

that the PUJ dynamical model can accurately predict the dynamical motion of the soft arm in 3D space considering the viscoelasticity of the arm.

The main contributions of this paper enlist:

- We introduce a new modeling methodology for soft robot arms under a Piecewise Universal Joint (PUJ) assumption which can handle situations that PCC can not, such as gravity and external forces.
- We develop a kinematic model based on PUJ and experimentally verify superior modeling accuracy over the PCC model. The maximum position/rotation error of the PUJ model is 6.7x/4.6x lower than the PCC model.
- We devise a dynamical model based on PUJ and experimentally validate it on a 3D soft arm with four segments in a variety of operational scenaria.

II. KINEMATICS

In this section, we introduce a kinematic model for soft robotic arms, which maps the soft arm directly to a discrete joint robot.

A. Modeling Assumptions

A soft robotic arm that operates in the 3D space is usually composed of multiple independently actuated segments, that can typically bend on a plane without torsional deformation. This characteristic serves as the chief modeling assumption in this paper. Under this assumption, the motion characteristics of a soft robotic arm are very similar to a rigid serial link mechanism, i.e., a universal joint. A universal joint (also called Cardan joint or Hooke's joint) is a compound joint whose two axes are orthogonal [16]. Universal joints are often used in the design of redundant robots and continuum robots to achieve semi-soft flexible motion [6], [17]. In this paper, we capitalize on this assumption, termed PUJ, to model the kinematics and dynamics of a soft robotic arm in 3D as a series of universal joints.

B. Kinematics Based on Piecewise Universal Joint

Consider a soft arm composed of n-segment. We denote the reference coordinate systems at the base of the arm and the ends of each segment as $\{S_0\}, \ldots, \{S_n\}$, as illustrated in Figure 2(a). We use these coordinate systems to represent the state of the soft arm. We abstract the kinematics via a homogeneous transformation matrix $\mathbf{T}_{i-1}^{i} \in \mathbb{R}^{4\times4}$ (see [16, Chapter 2]) between consecutive coordinate systems, given by:

$$\mathbf{T}_{i-1}^{i} = \begin{bmatrix} \mathbf{R}_{i-1}^{i} & \mathbf{p}_{i-1}^{i} \\ (0,0,0) & 1 \end{bmatrix}, \tag{1}$$

where $\mathbf{R}_{i-1}^{i} \in \mathbb{R}^{3\times3}$ is a rotation matrix and $\mathbf{p}_{i-1}^{i} \in \mathbb{R}^{3}$ is a translation (column) vector. It follows that the forward kinematics of soft robotic arm with n-segment is given by the product of the segment transformation matrices as:

$$\mathbf{T}_{0}^{n} = \prod_{i=1}^{n} \mathbf{T}_{i-1}^{i}. \tag{2}$$

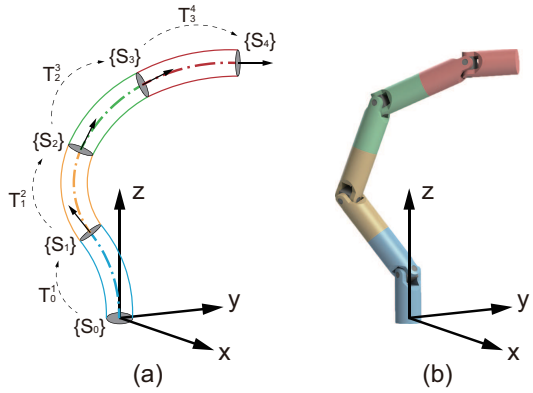

Fig. 2. An illustration of a soft robotic arm alongside its equivalent rigid robotic representation in 3D space. (a) The kinematic representation of a four-segment soft robotic arm, where reference frame S_0 is attached at the robot's base, and S_i is attached at the end of the i-th segment. The homogeneous transformation $\mathbf{T}_{i-1}^{i}$ maps S_{i-1} to S_i. (b) An equivalent representation of the soft manipulator based on PUJ.

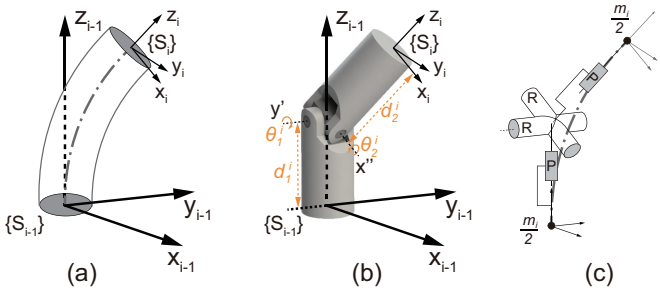

Fig. 3. Equivalent representation of the i-th segment of the soft robotic arm. (a) An illustration of a single segment of the soft arm: S_{i-1} and S_i are the two coordinate frames attached at both ends of the segment. (b) A kinematic representation based on a universal joint: translation lengths d_1^i, d_2^i and rotation angles θ_1^i, θ_2^i are chosen as the configuration variables. (c) Two prismatic joints P and two revolute joints R are used to imitate the movement of the segment. The mass of a single segment m_i is evenly distributed to both ends of the segment, while the mass of other elements is regarded as zero.

$\mathbf{T}_{i-1}^{i}$ transforms vectors from the i-th coordinate frame to the $(i-1)$-th, thus $\mathbf{T}_{0}^{n}$ serves to express the end effector in the arm base coordinate frame.

The n-segment soft robotic arm is equivalently represented by n serial universal joints (Figure 2(b)). Taking the i-th segment for illustration, we showcase how to select the configuration variables for the universal joint, and proceed to provide the expression for the homogeneous transformation matrix of the i-th segment.

The tuple $(d_1^i, \theta_1^i, \theta_2^i, d_2^i)$ represents the configuration variables for the i-th segment. The coordinate system S_i fixed at the tip of the i-th segment is obtained from S_{i-1} via a sequence of four operations: 1) translation along the z-axis by d_1^i, 2) rotation around the y-axis by θ_1^i, 3) rotation around the x-axis by θ_2^i, and 4) translation along the z-axis by d_2^i (see Figure 3(b)). The homogeneous transformation matrix for the i-th segment can be written as:

$$\mathbf{T}^i_{i-1} = \mathbf{Trans}(\mathbf{z}, d^i_1)\mathbf{Rot}(\mathbf{y}, \theta^i_1)\mathbf{Rot}(\mathbf{x}, \theta^i_2)\mathbf{Trans}(\mathbf{z}, d^i_2)$$
$$= \begin{bmatrix} c_{\theta^i_1} & s_{\theta^i_1}s_{\theta^i_2} & s_{\theta^i_1}c_{\theta^i_2} & d^i_2 s_{\theta^i_1}c_{\theta^i_2} \\ 0 & c_{\theta^i_2} & -s_{\theta^i_2} & -d^i_2 s_{\theta^i_2} \\ -s_{\theta^i_1} & c_{\theta^i_1}s_{\theta^i_2} & c_{\theta^i_1}c_{\theta^i_2} & d^i_1 + d^i_2 c_{\theta^i_1}c_{\theta^i_2} \\ 0 & 0 & 0 & 1 \end{bmatrix}, \quad (3)$$

where $\mathbf{Trans} \in \mathbb{R}^{4\times4}$ denotes the homogeneous transformation matrix of translation along an axis, $\mathbf{Rot} \in \mathbb{R}^{4\times4}$ denotes the homogeneous transformation matrix of rotation around an axis as defined in [16, Section 2.2], and c_θ, s_θ respectively abbreviate $\cos\theta$, $\sin\theta$.

C. State Estimation

In this part, we consider the inverse problem, i.e., how to estimate the configuration variables from the posture of the reference coordinate systems. The postures $\{S_0\}, ..., \{S_n\}$ are usually measured from sensors such as cameras. The 3x3 upper left block in (3) is the measured rotation matrix $\mathbf{R}^i_{i-1}$ and the 3x1 upper right block is the measured translation vector $\mathbf{p}^i_{i-1}$. Angles θ^i_1 and θ^i_2 can be derived by converting the measured rotation matrix to the form of Z-Y-X Euler angles $(\alpha, \beta, \gamma)^\top$. For a universal joint, $\alpha = 0$, $\beta = \theta^i_1$, and $\gamma = \theta^i_2$. This procedure is rather standard using software packages (e.g., $rotm2eul$ in Matlab) and is not detailed here, for length considerations. Note that for Z-Y-X Euler angles, a singularity occurs when the second Euler angle $\beta = \pm90°$ (Section 2.2 of [16]). Therefore, to apply the PUJ model on soft robotic arms it is sufficient that the single segment not bend beyond $90°$, which is consistent with our design of the soft robotic arm. The translation lengths d^i_1 and d^i_2 can be derived from the measured translation vector $\mathbf{p}^i_{i-1} = (x^i_{i-1}, y^i_{i-1}, z^i_{i-1})^\top$ as follows:

$$\begin{cases} d^i_2 = \frac{y^i_{i-1}}{-s_{\theta^i_2}}, d^i_1 = z^i_{i-1} - d^i_2 c_{\theta^i_1}c_{\theta^i_2}, & \theta^i_2 > \epsilon \\ d^i_2 = \frac{x^i_{i-1}}{s_{\theta^i_1}c_{\theta^i_2}}, d^i_1 = z^i_{i-1} - d^i_2 c_{\theta^i_1}c_{\theta^i_2}, & \theta^i_1 > \epsilon \;\&\; \theta^i_2 < \epsilon \\ d^i_1 = d^i_2 = \frac{z^i_{i-1}}{1+c_{\theta^i_1}c_{\theta^i_2}}, & \theta^i_1 < \epsilon \;\&\; \theta^i_2 < \epsilon \end{cases}. \quad (4)$$

We set $\epsilon = 0.05rad$ in this paper. When the configuration of the segment is almost straight ($\theta^i_1 < \epsilon$ & $\theta^i_2 < \epsilon$), the two translation axes coincide, which causes the contribution of these two degrees of freedom to the end effector motion to be indistinguishable. In order to achieve a robust method for state estimation, we use the last term of $\mathbf{p}^i_{i-1}$ to obtain d^i_1 and d^i_2 with the constraint that $d^i_1 = d^i_2$ in this scenario.

D. Exponential Coordinate Representation

Exponential coordinate representation is the most intuitive and convenient way to describe rigid-body motions; we adopt this to describe the kinematics and dynamics of the serial universal joints. For brevity, we provide the overview here with a detailed description accessible at [18, Chapter 3].

The forward kinematics of n serial universal joints can be represented by the product of exponentials (PoE) [19]:

$$\mathbf{T}(\mathbf{q}) = e^{[\boldsymbol{S}_1]q_1} \cdots e^{[\boldsymbol{S}_n]q_n}\mathbf{H}, \quad (5)$$

where $\mathbf{q} := (d^i_1, \theta^1_1, \theta^1_2, d^1_2 \ldots, d^n_1, \theta^n_1, \theta^n_2, d^n_2)^\top \in \mathbb{R}^{4n}$ is the collection of all configuration variables; $\mathbf{T}(\mathbf{q}) \in \mathbb{R}^{4\times4}$ is the pose of the end effector; $\mathbf{H} \in \mathbb{R}^{4\times4}$ is the pose of the end-effector when all configuration variables of the arm are zero (zero position); $\boldsymbol{S}_i$ is the normalized screw axis of joint i as expressed in the fixed base frame, with $\boldsymbol{S}_i$ given by:

$$[\boldsymbol{S}_i] = \begin{bmatrix} [\boldsymbol{\omega}_i] & \mathbf{v}_i \\ (0,0,0) & 0 \end{bmatrix}, [\boldsymbol{\omega}_i] = \begin{bmatrix} 0 & -\omega^i_3 & \omega^i_2 \\ \omega^i_3 & 0 & -\omega^i_1 \\ -\omega^i_2 & \omega^i_1 & 0 \end{bmatrix}. \quad (6)$$

If joint i is revolute, $\boldsymbol{\omega}_i := (\omega^i_1, \omega^i_2, \omega^i_3)^\top$ is a unit vector along the positive direction of the joint axis and $\mathbf{v}_i$ is the velocity of the point that coincides with the base coordinate system when the joint rotates in an angular velocity of $||\boldsymbol{\omega}_i||$. If joint i is prismatic, $\boldsymbol{\omega}_i = (0,0,0)^\top$, $\mathbf{v}_i := (v^i_1, v^i_2, v^i_3)^\top$ is a unit vector along the positive direction of joint axis. Table I lists the screw axis for a single universal joint as an example.

TABLE I
SCREW AXES $\boldsymbol{S}_i$ FOR ONE UNIVERSAL JOINT

i	ω_i	$\mathbf{v}_i$
1	$(0,0,0)^\top$	$(0,0,1)^\top$
2	$(0,1,0)^\top$	$(-d_0,0,0)^\top$
3	$(1,0,0)^\top$	$(0,d_0,0)^\top$
4	$(0,0,0)^\top$	$(0,0,1)^\top$

d_0 is the initial length of the first link of the universal joint when at its zero position.

Unlike the commonly used Denavit–Hartenberg representation [20], the product of exponentials representation has the advantage that no link reference frames need to be explicitly defined, resulting in simple and intuitive equations for kinematics and dynamics [21].

III. DYNAMICS

The dynamical characterization is of great importance for the design, analysis, and control of soft robotic arms. In this section, we introduce a dynamical model based on the PUJ model introduced in the prequel. The dynamical model is derived from rigid-body dynamics. We take the viscoelasticity of the soft arm into consideration by adding the elastic and damping term into the dynamical equations. This methodology bears the advantage that the well-established dynamical system modeling and analysis for rigid-body robots now carries to soft robotic arms.

As the first step to model the dynamics of the soft arm under PUJ, we assume that the length of each universal joint remains constant during operation. This means that an n-segment soft robotic arm is represented by n serial universal joints, each one comprising of two revolute joints, for a total of $2n$ joints (see Figure 2(b)). We further make a simplifying approximation assuming that the mass of the segment is evenly distributed at both ends as two equal point

masses, cf. Figure 3(c): this mass distribution ensures that the mass of the arm is distributed on the central axis of the soft arm.

The general form of the dynamics for a rigid robot are captured by [16]:

$$\mathbf{M}(\mathbf{q})\ddot{\mathbf{q}} + \mathbf{C}(\mathbf{q}, \dot{\mathbf{q}})\dot{\mathbf{q}} + \mathbf{G}(\mathbf{q}) = \boldsymbol{\tau},$$

where $\mathbf{q} := (\theta_1^1, \theta_2^1, \ldots, \theta_1^n, \theta_2^n)^\top \in \mathbb{R}^{2n}$, $\mathbf{M}(\mathbf{q}) \in \mathbb{R}^{2n\times 2n}$ is the inertia matrix, $\mathbf{C}(\mathbf{q}, \dot{\mathbf{q}}) \in \mathbb{R}^{2n\times 2n}$ is the matrix capturing the Coriolis and centrifugal terms, $\mathbf{G}(\mathbf{q}) \in \mathbb{R}^{2n}$ is the gravity term, and $\boldsymbol{\tau} \in \mathbb{R}^{2n}$ is the torque applied to each joint.

There are several methods to obtain the rigid body dynamical model, such as Lagrange dynamics [14], Newton-Euler method [22], TMT methods [23], and more. In our work, we invoke the Newton-Euler recursive method which is computationally efficient and most suitable for deriving the equivalent model of a soft robotic arm with many degrees of freedom. We derive the dynamics based on the screw theory. For the detailed derivation process, we refer the reader to [18, Chapter 8].

Soft robotic arms are usually made of materials that exhibit unignorable viscoelasticity. As a consequence, the rigid body model fails to fully describe the motion characteristics of the soft arm. For this reason, we augment the model by adding an elastic and damping term, so as to describe the soft arm as a rigid joint robot with joint viscoelasticity. We only consider first-order viscoelasticity in this paper as in [10], that is, elastic and damping is captured by two linear terms $\mathbf{Kq}$ and $\mathbf{D}\dot{\mathbf{q}}$, respectively. The complete dynamical equation is:

$$\mathbf{M}(\mathbf{q})\ddot{\mathbf{q}} + \mathbf{C}(\mathbf{q}, \dot{\mathbf{q}})\dot{\mathbf{q}} + \mathbf{G}(\mathbf{q}) + \mathbf{Kq} + \mathbf{D}\dot{\mathbf{q}} = \boldsymbol{\tau}, \qquad (7)$$

where $\mathbf{K} \in \mathbb{R}^{2n\times 2n}$ is a diagonal stiffness matrix and $\mathbf{D} \in \mathbb{R}^{2n\times 2n}$ is a diagonal damping matrix. The procedure to estimate these matrices is detailed in the next section.

IV. SOFT ROBOTIC ARM

In this section, we introduce the pneumatic soft robotic arm system. We first describe the soft arm and control system and proceed to analyze the mapping between the pneumatic pressure and torque. Last but not least, we introduce a mechanism for system identification, i.e., for learning the parameters in (7), which is verified in the experimental section.

A. Soft Arm System

We use a soft robotic arm developed in our previous work [2] to validate the proposed models (see Figure 4). The design, fabrication, and simulation optimization methods of the soft Honeycomb Pneumatic Network Arm are detailed in [24]. The arm consists of four independent actuated segments and is actuated by a total of 16 proportional valves. We placed reflective markers on both ends of each segment of the arm, and use MCS (Motion Capture System) to obtain the pose of the markers. The arm is $66cm$ long and exhibits a maximum load capacity of $3kg$, with $4kg$ self-weight, and is capable of flexible motion in 3D space.

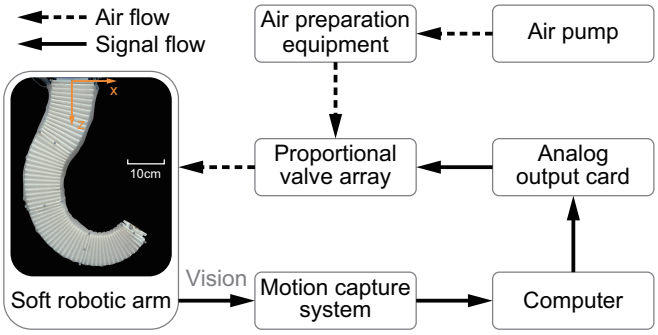

Fig. 4. The soft robotic arm and accompanying hardware system for the validation of the proposed models.

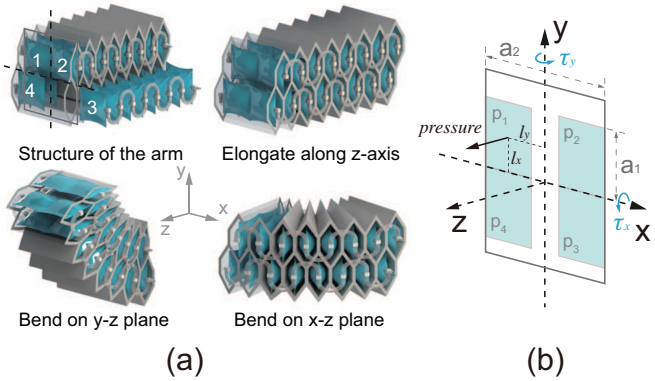

Fig. 5. Structure of the pneumatically actuated soft robotic arm. (a) Design and 3D deformation of a segment of the soft robotic arm. (b) The cross-section of the soft robotic arm and the schematic diagram of the airbag distribution.

B. Torque To Pressure Mapping

In order to apply (7) to the pneumatic soft robotic arm, it is imperative to devise a conversion mapping between the air pressure of the soft arm and the torque of the equivalent model. The structure of the soft arm is shown in Figure 5(a). Four groups of airbags are placed side by side in the honeycomb structure. The air pressures of the four airbags are denoted by p_1, p_2, p_3, p_4. We adopt the assumption $p_1+p_4 = p_2+p_3$, which corresponds to reducing the internal consumption pertaining to the driving forces. We apply the following decomposition:

$$\begin{bmatrix} p_1 & p_2 \\ p_3 & p_4 \end{bmatrix} = \begin{bmatrix} p_z & p_z \\ p_z & p_z \end{bmatrix} + \begin{bmatrix} p_x & p_x \\ 0 & 0 \end{bmatrix} + \begin{bmatrix} p_y & 0 \\ p_y & 0 \end{bmatrix}, \qquad (8)$$

where p_x, p_y respectively correspond to the air pressure component that causes the bending around the x and y axes, and p_z is the air pressure component that causes the elongation along the z axis. We relate the air pressure components with the produced force and torque using the formulas $F = pS$, and $\tau = lF$:

$$F_z = 4p_z s, \quad \tau_x = 2p_x s l_x, \quad \tau_y = 2p_y s l_y, \qquad (9)$$

where s is the average contact area between an airbag and the honeycomb structure and $l_x = \frac{a_1}{2}$, $l_y = \frac{a_2 - a_1}{2}$ are the

average distances that generate torque around the x and y axes, as shown in Figure 5(b). Note that the contact area between the airbag and the honeycomb structure may vary with pressure. For this reason, we carried some preliminary experiments to determine the average contact area s. Table II lists the design parameters of the four-segment soft robotic arm.

TABLE II
DESIGN PARAMETERS OF THE SOFT ROBOTIC ARM

Segment	Length of segment[cm]	Mass of segment[kg]	Width of structure a_2[cm]	Width of airbag a_1[cm]
1 (base)	18.5	1.2	11	4.5
2	17.5	0.8	10	4.0
3	15.5	0.6	9	3.5
4 (tip)	14.5	0.4	8	3.0

C. System Identification

We desscribe how to estimate parameters $\mathbf{M}, \mathbf{C}, \mathbf{G}, \mathbf{K}$, and $\mathbf{D}$ in (7). The matrices $\mathbf{M}$, $\mathbf{C}$, and $\mathbf{G}$ are related to the mass and geometric length of the equivalent rigid links, which can be calculated by measuring the mass and the initial length of the soft arm (as listed in Table II). For the detailed recursive calculation process, we refer the reader to [18, Section 8.3]. The stiffness coefficient $\mathbf{K}$ and the damping coefficient $\mathbf{D}$ are obtained from experimentally collected data by using linear regression as follows. Note that (7) can be equivalently written as $\mathbf{K}\mathbf{q}+\mathbf{D}\dot{\mathbf{q}} = \boldsymbol{\tau} - \mathbf{M}(\mathbf{q})\ddot{\mathbf{q}} - \mathbf{C}(\mathbf{q},\dot{\mathbf{q}})\dot{\mathbf{q}} - \mathbf{G}(\mathbf{q})$, where the left side contains the terms to be identified and the right side can be computed from data, along with the previously identified matrices $\mathbf{M}, \mathbf{C}, \mathbf{G}$. For collecting data, we raise the tip of the soft arm, then let the arm swing freely under gravity ($\boldsymbol{\tau} = 0$). In this process, we record the posture of the arm. The data were collected at a frequency of 100Hz, and values of $\mathbf{q}$, $\dot{\mathbf{q}}$, and $\ddot{\mathbf{q}}$ need to be measured for identification. We use the state estimation method introduced in Section II.C to obtain the configuration variables $\mathbf{q} = (\theta_1^1, \theta_2^1, \ldots, \theta_1^n, \theta_2^n)^\top$ from the arm postures. Based on the natural response in (7), we fit measurements $\mathbf{q}$ to the function $ae^{-bt}\sin(\omega t - c)$, which allows for both denoising and robust computation of the derivatives $\dot{\mathbf{q}}$ and $\ddot{\mathbf{q}}$.

In view of the structural property of the soft arm used in this paper, we identify the stiffness ($N\,m\,rad^{-1}$) and damping ($N\,m\,s\,rad^{-1}$) across the x and y axes separately. The identification results are:

$$\mathbf{K} = diag(3.90, 3.58, 3.08, 2.71, 2.25, 2.20, 0.81, 0.88)$$
$$\mathbf{D} = diag(0.25, 0.19, 0.16, 0.10, 0.06, 0.06, 0.03, 0.02).$$

V. EXPERIMENTS

A. Kinematic Performance

To demonstrate the performance of the proposed PUJ model and compare it with the PCC model, we conducted the following experiment. A 500g weight was added to the tip of the arm, and we gradually increased the air pressure from 0 (zero position) to $2.5bar$ to bend all sections of the arm on the $x = 0$ plane. We used the MCS to obtain the posture of the markers on the arm. The measured postures are then converted to the configuration parameters (ϕ, l, κ) of the PCC model (see [7]) and the configuration parameters $(d_1, \theta_1, \theta_2, d_2)$ of the universal joint model, as elaborated in Section II.C. After calculating the configuration parameters, the forward kinematics of the PUJ model is calculated using (5). The position and rotation errors are calculated by comparing the calculated forward kinematics with the posture of the end effector obtained by the MCS. The results are illustrated in Figure 6: the universal joint model performs globally better than the PCC model. As the deformation of the arm increases, the gravitational moment of the load continues to increase, whence the deviation of the PCC model also increases. The maximum position/rotation error of the PCC model is 6.7x/4.6x higher than the PUJ model. It is noteworthy that the error of our proposed PUJ model does not scale with pressure: this is a positive attribute especially when the soft arm is used in scenes where external forces cannot be ignored, such as daily interactive tasks. .

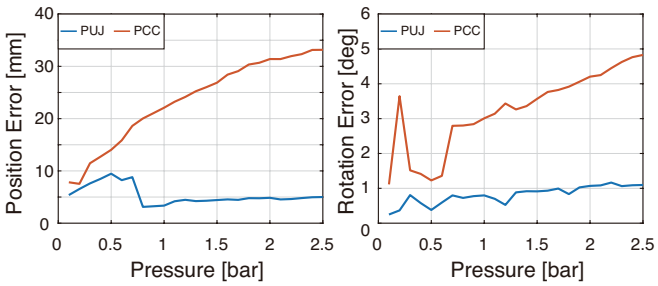

Fig. 6. Comparison of kinematic modeling performance between piecewise constant curvature (PCC) model and piecewise universal joint (PUJ) model. The arm bends on the $x = 0$ plane.

B. Dynamic Response (1): Free Swing

The first dynamic experiment is used to verify the validity of the proposed model and the accuracy of system identification. The actuation pressure in this experiment is equal to zero, and our PUJ model is used to predict the motion of the arm. In the experiment, we raised the arm in the $x = 0$ plane and recorded the configuration variables at $t = 0s$ as the initial state of the PUJ model for the numerical evaluation of our model. We then let the arm swing freely under gravity, record its motion, and identify the configuration variables as explained in the previous section. We carried out two experiments: a) without load and b) under $200g$ load at the end effector. The numerical simulation of forward dynamics based on (7) is implemented in Matlab based on the package provided by [18]. As it can be seen from the experimental results in Figure 7, our proposed model exhibits high accuracy. The average joint angle errors are $0.57°$ and $1.1°$ for the experiments without and with load, respectively. Note that the proposed PUJ model can accurately capture the characteristics of the imperfect sinusoidal decay motion of the distal segment of the arm (Figure 7(a)) as well as it predicts the motion characteristics of the arm well when the

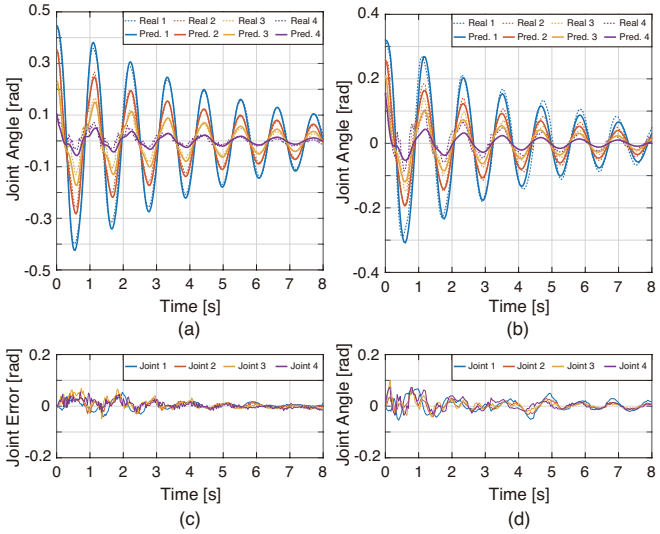

Fig. 7. Free swing experiments. The arm is swinging freely under gravity (a) without load on the tip; (b) with a $200g$ load on the tip. Solid lines illustrate model predictions and dashed lines real data. Errors between model predictions and real data are shown in (c) and (d).

tip is loaded (Figure 7(b)).

C. Dynamic Response (2): Step Response

The second dynamic experiment is used to verify the validity of the proposed model for excitation with a step response. We conducted three experiments (as shown in Figure 8): on-plane motion (all segments bend on the $x = 0$ plane), out-of-plane motion (the first two segments bend on the $y = 0$ plane and the last two on the $x = 0$ plane) without load, and out-of-plane motion with a $200g$ load on the tip. Initially, the arm is in the zero position. At $t = 0s$, certain segments of the arm are provided with $2bar$ pressure step inputs as excitation to generate on-plane/out-of-plane motion, and the pressure is maintained throughout the experiments. The responses of the real soft arm and the model-based simulated response are recorded for all three experiments.

The results attest to the accuracy of PUJ. For on-plane motion, the average joint error is $1.6°$, and the maximum joint steady-state error is $2.2°$. For out-of-plane motion, the average joint error is $2.1°$, and the maximum joint steady-state error is $7.9°$. For out-of-plane motion with load, the average joint error is $2.5°$, and the maximum joint steady-state error is $9.3°$. It can be observed that the fourth joint has the largest steady-state error (see Figure 8(b), (c)), which is attributed to the axial torsion of the arm when performing the out-of-plane motion. In addition, for these test scenarios, our model predicts a more oscillatory behavior than the arm actually demonstrates, which may be explained in view of the fact that our model assumes the arm as a series of inextensible universal joints. When pressured, the arm will extend, causing the parameters to deviate from the real arm dynamical parameters. Our future work will develop dynamical models for extensible arms based on the universal joint.

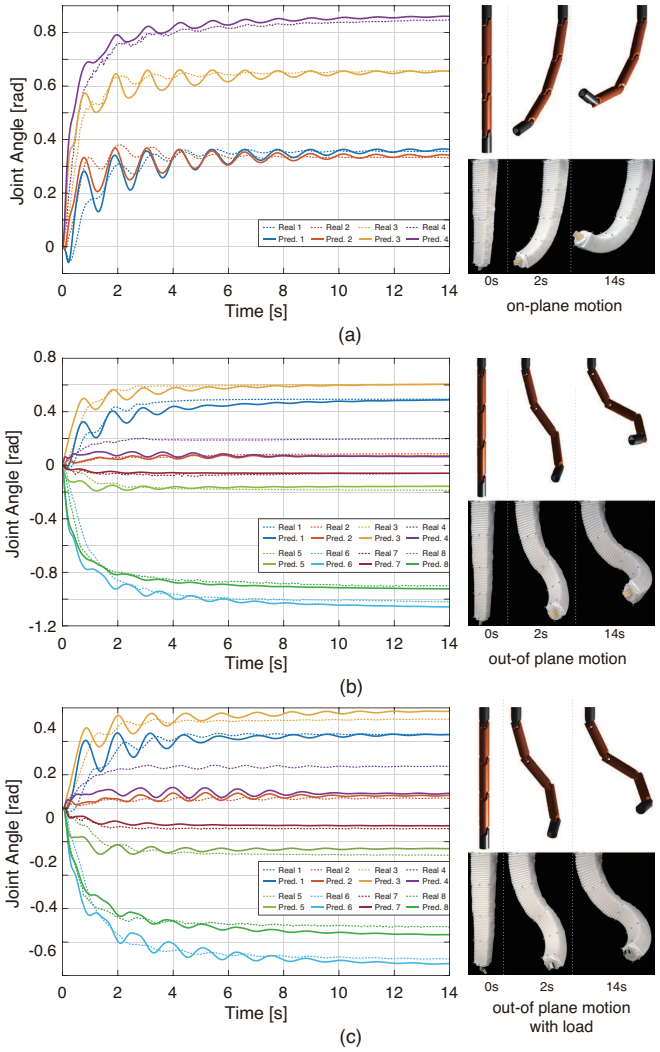

Fig. 8. Step response experiments. (a) The dynamic response of on-plane motion. (b) The dynamic response of out-of-plane motion without load. (c) The dynamic response of out-of-plane motion with 200g load on the tip. Snapshots (t=0, 2, 14s) of experiments are shown on the right. Solid lines illustrate model predictions and dashed lines real data.

VI. CONCLUSIONS AND DISCUSSION

We devised and tested a new kinematic and dynamical model for a soft arm in 3D space in the presence of gravity and external load. The PUJ model proposed in this paper improves the predictive accuracy in the presence of external forces by relaxing the constraints of constant curvature deformation in PCC. The universal joint is not the only way to represent a non-constant curvature deformation of soft arms. For example, the model in [15] can be extended to represent a non-constant curvature deformation of soft arms. In future work, we plan to capitalize the developed model for controlling the soft arm.

ACKNOWLEDGMENT

We would like to thank Hao Jiang, Yusong Jin, and Yinghao Gan for fruitful discussions.

REFERENCES

[1] S. Kim, C. Laschi, and B. Trimmer, "Soft robotics: a bioinspired evolution in robotics," *Trends in biotechnology*, vol. 31, no. 5, pp. 287–294, 2013.

[2] H. Jiang, Z. Wang, Y. Jin, X. Chen, P. Li, Y. Gan, S. Lin, and X. Chen, "Hierarchical control of soft manipulators towards unstructured interactions," *The International Journal of Robotics Research*, vol. 40, no. 1, pp. 411–434, 2021.

[3] M. Cianchetti, T. Ranzani, G. Gerboni, I. De Falco, C. Laschi, and A. Menciassi, "Stiff-flop surgical manipulator: Mechanical design and experimental characterization of the single module," in *IEEE/RSJ International Conference on Intelligent Robots and Systems*, 2013, pp. 3576–3581.

[4] P. H. Nguyen, C. Sparks, S. G. Nuthi, N. M. Vale, and P. Polygerinos, "Soft poly-limbs: Toward a new paradigm of mobile manipulation for daily living tasks," *Soft Robotics*, vol. 6, no. 1, pp. 38–53, 2019.

[5] D. Rus and M. T. Tolley, "Design, fabrication and control of soft robots," *Nature*, vol. 521, pp. 467–475, 2015.

[6] M. W. Hannan and I. D. Walker, "Kinematics and the implementation of an elephant's trunk manipulator and other continuum style robots," *Journal of Robotic Systems*, vol. 20, no. 2, pp. 45–63, 2003.

[7] R. J. Webster III and B. A. Jones, "Design and kinematic modeling of constant curvature continuum robots: A review," *The International Journal of Robotics Research*, vol. 29, no. 13, pp. 1661–1683, 2010.

[8] A. D. Marchese and D. Rus, "Design, kinematics, and control of a soft spatial fluidic elastomer manipulator," *The International Journal of Robotics Research*, vol. 35, no. 7, pp. 840–869, 2016.

[9] A. D. Marchese, R. Tedrake, and D. Rus, "Dynamics and trajectory optimization for a soft spatial fluidic elastomer manipulator," *The International Journal of Robotics Research*, vol. 35, no. 8, pp. 1000–1019, 2016.

[10] C. Della Santina, R. K. Katzschmann, A. Bicchi, and D. Rus, "Model-based dynamic feedback control of a planar soft robot: trajectory tracking and interaction with the environment," *The International Journal of Robotics Research*, vol. 39, no. 4, pp. 490–513, 2020.

[11] R. K. Katzschmann, C. Della Santina, Y. Toshimitsu, A. Bicchi, and D. Rus, "Dynamic motion control of multi-segment soft robots using piecewise constant curvature matched with an augmented rigid body model," in *IEEE International Conference on Soft Robotics*, 2019, pp. 454–461.

[12] F. Renda, F. Boyer, J. Dias, and L. Seneviratne, "Discrete cosserat approach for multisection soft manipulator dynamics," *IEEE Transactions on Robotics*, vol. 34, no. 6, pp. 1518–1533, 2018.

[13] C. Della Santina, A. Bicchi, and D. Rus, "On an improved state parametrization for soft robots with piecewise constant curvature and its use in model based control," *IEEE Robotics and Automation Letters*, vol. 5, no. 2, pp. 1001–1008, 2020.

[14] I. S. Godage, G. A. Medrano-Cerda, D. T. Branson, E. Guglielmino, and D. G. Caldwell, "Dynamics for variable length multisection continuum arms," *The International Journal of Robotics Research*, vol. 35, no. 6, pp. 695–722, 2016.

[15] C. Wang, C. G. Frazelle, J. R. Wagner, and I. D. Walker, "Dynamic control of multisection three-dimensional continuum manipulators based on virtual discrete-jointed robot models," *IEEE/ASME Transactions on Mechatronics*, vol. 26, no. 2, pp. 777–788, 2020.

[16] B. Siciliano and O. Khatib, *Springer Handbook of Robotics*, 2016.

[17] A. Yeshmukhametov, K. Koganezawa, and Y. Yamamoto, "Design and kinematics of cable-driven continuum robot arm with universal joint backbone," in *IEEE International Conference on Robotics and Biomimetics*, 2018, pp. 2444–2449.

[18] K. M. Lynch and F. C. Park, *Modern Robotics*, 2017.

[19] R. W. Brockett, "Robotic manipulators and the product of exponentials formula," in *Mathematical Theory of Networks and Systems*, 1984, pp. 120–129.

[20] J. Denavit and R. S. Hartenberg, "A kinematic notation for lower-pair mechanisms based on matrices," *ASME Journal of Applied Mechanics*, vol. 22, no. 2, pp. 215–221, 1955.

[21] R. Featherstone, *Rigid Body Dynamics Algorithms*, 2014.

[22] J. Jung, R. S. Penning, N. J. Ferrier, and M. R. Zinn, "A modeling approach for continuum robotic manipulators: Effects of nonlinear internal device friction," in *IEEE/RSJ International Conference on Intelligent Robots and Systems*, 2011, pp. 5139–5146.

[23] S. H. Sadati *et al.*, "TMTDyn: A Matlab package for modeling and control of hybrid rigid–continuum robots based on discretized lumped systems and reduced-order models," *The International Journal of Robotics Research*, vol. 40, no. 1, pp. 296–347, 2021.

[24] H. Jiang, X. Liu, X. Chen, Z. Wang, Y. Jin, and X. Chen, "Design and simulation analysis of a soft manipulator based on honeycomb pneumatic networks," in *IEEE International Conference on Robotics and Biomimetics*, 2016, pp. 350–356.